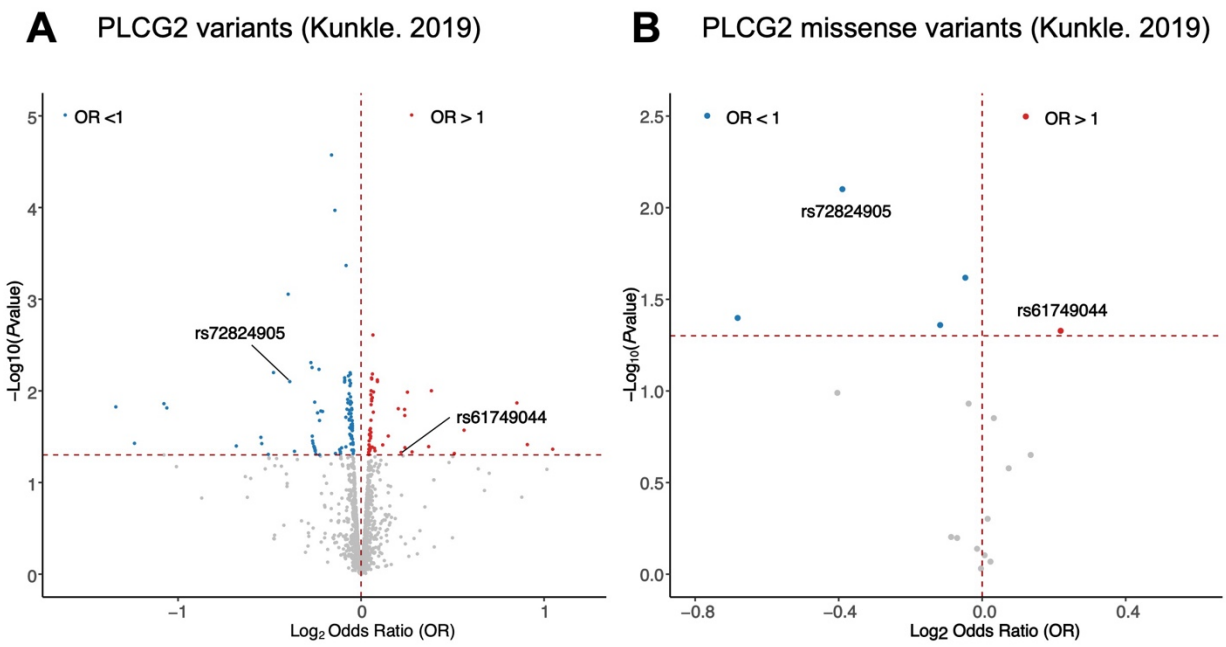

C

Variant		
PLCG2 M28L (rs61749044)		
OR	*p*-value	Dataset
1.16	0.047	Kunkle. 2019
1.25	0.054	Olive. 2020
1.16	0.18	Schwarzentruber. 2021
1.01	0.64	Bellenguez. 2022

Variant		
PLCG2 P522R (rs72824905)		
OR	*p*-value	Dataset
0.76	0.007	Kunkle. 2019
0.63	0.002	Olive. 2020
0.76	6.00E-06	Schwarzentruber. 2021
0.74	2.60E-10	Bellenguez. 2022

Figure S1. The association between PLCG2 variants and AD risk (related to Figure 1)

(A) Volcano plot shows the relationship between the p-value and odds ratio of PLCG2 variants. **(B)** Volcano plot shows the relationship between the p-value and odds ratio of PLCG2 missense variants. **(C)** Tables show OR and the p-value from reported GWAS of late-onset AD datasets.

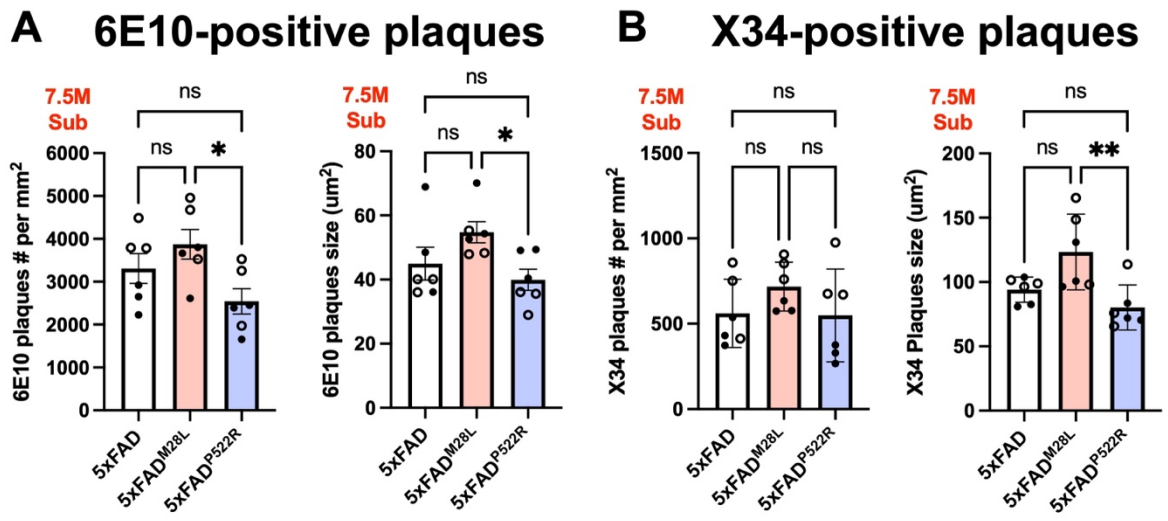

Figure S2. Numbers and sizes of 6E10-positive and X34-positive plaques in AD mice (related to Figure 2)

(A) Scatter plots show the quantification of the numbers and sizes of 6E10-positive plaques. **(B)** Scatter plots show the quantification of the numbers and sizes of X34-positive plaques. All data are expressed as the mean values ± SEM and analyzed by an ordinary one-way ANOVA and Tukey's multiple comparisons test (*P < 0.05, and **P < 0.01; ns: not significant). Male mice: •; female mice: o. n=6 per group; 3 male and 3 female mice; 6 experiments.

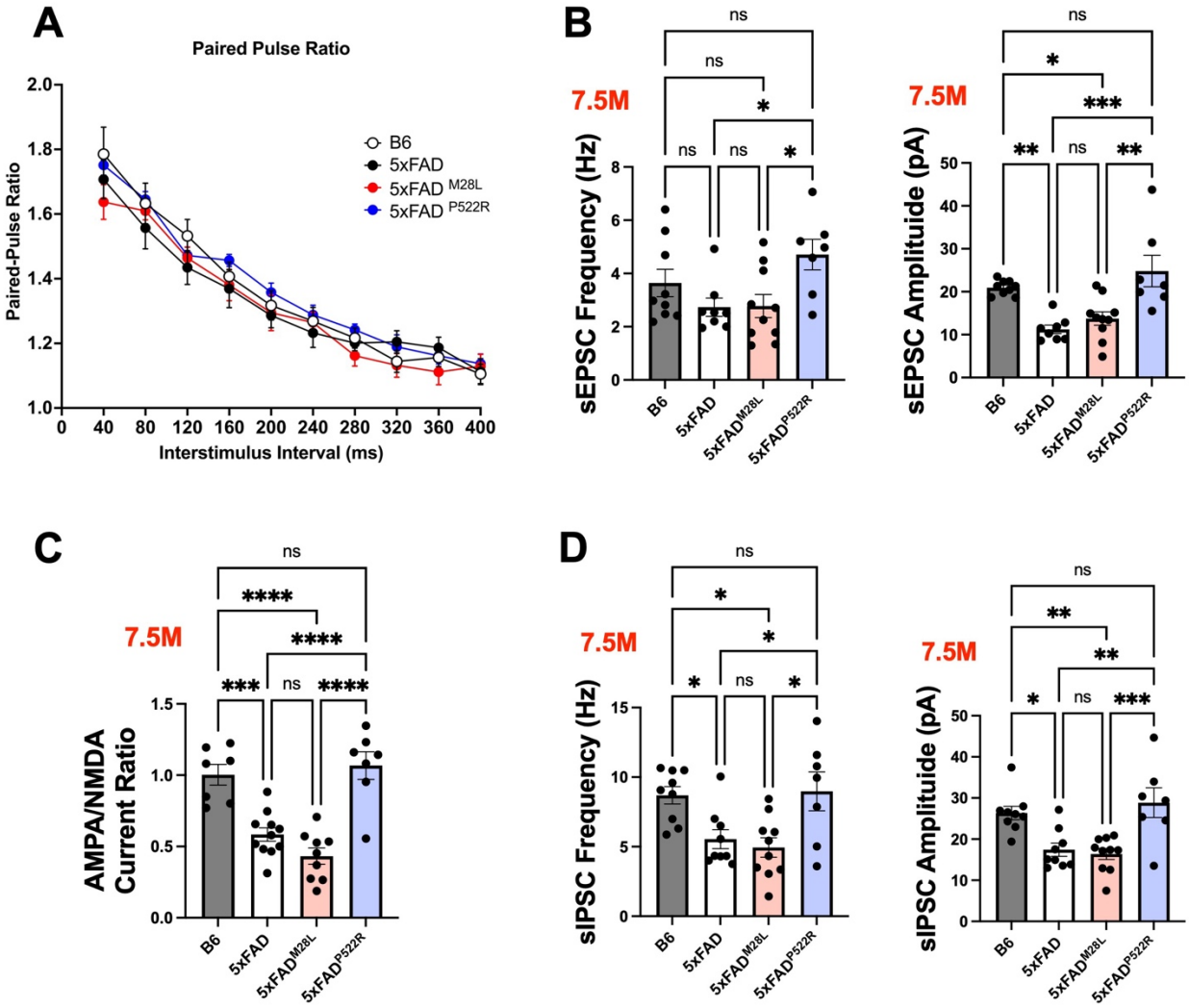
A
Paired Pulse Ratio
Paired-Pulse Ratio
Interstimulus Interval (ms)
B6
5xFAD
5xFAD M28L
5xFAD P522R
B
7.5M
sEPSC Frequency (Hz)
sEPSC Amplituide (pA)
C
AMPA/NMDA Current Ratio
D
sIPSC Frequency (Hz)
sIPSC Amplituide (pA)
ns

Figure S3. Paired-pulse ratios and whole-cell recordings in AD mice (related to Figure 4)

(A) Paired-pulse ratios were obtained every 20 s at 40 ms increasing inter-stimuli intervals, and no genotype differences were observed. **(B-D)** Whole-cell patch-clamp electrophysiological recordings were performed on hippocampal area CA1 pyramidal neurons. **(B)** Measures of spontaneous excitatory postsynaptic currents (sEPSCs) parameters (frequency and amplitude). **(C)** Measures of differences in excitatory transmission by measuring EPSCs mediated by AMPA and NMDA glutamate receptors. **(D)** Measures of sIPSC parameters (frequency and amplitude). The software pClamp11 (Molecular Devices) and MiniAnalysis (Synaptosoft) were used for quantification. Statistical analyses were performed using Prism (GraphPad Software). All data are presented as the mean ± SEM. * $P < 0.05$; ** $P < 0.01$; *** $P < 0.001$; **** $P < 0.0001$.

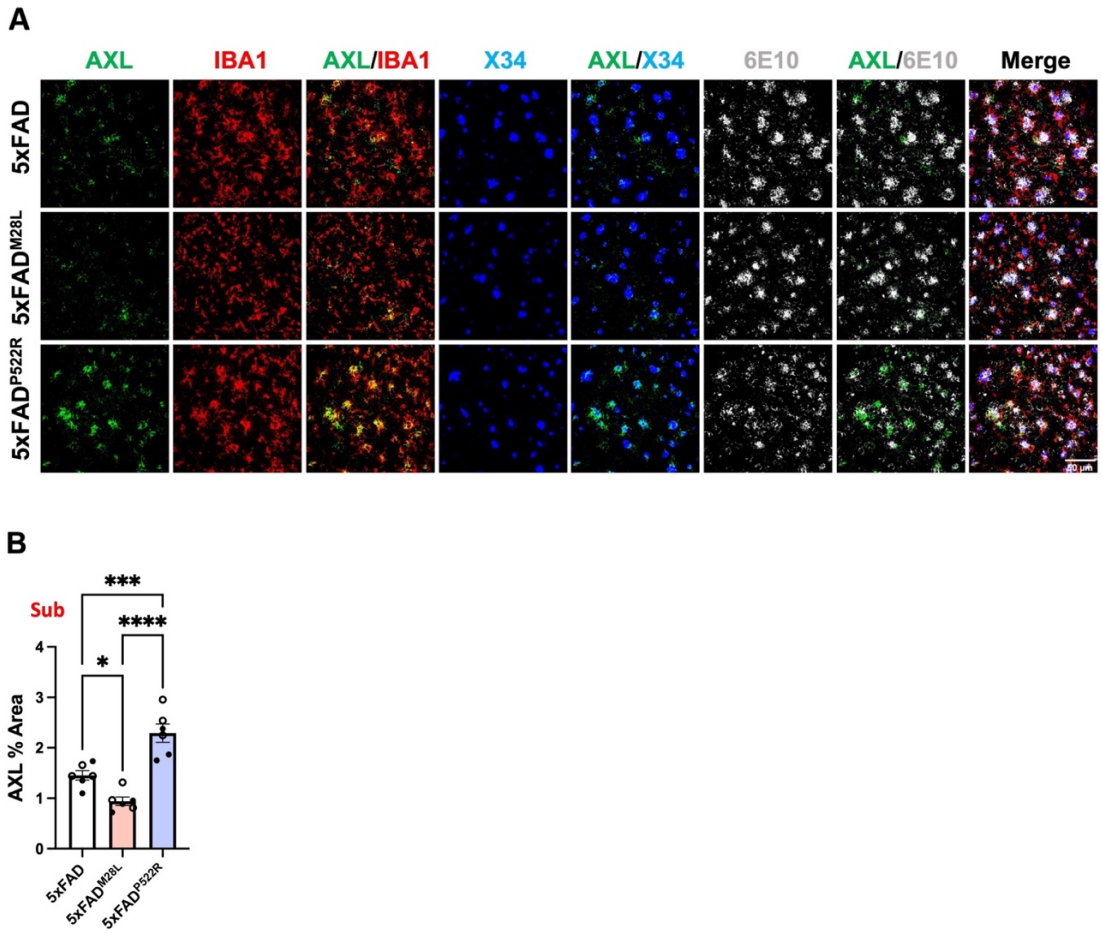

Figure S4. Microglial AXL expression level is mediated by PLCG2 variants in AD mice. (related to Figure 7)

(A) Representative images of microglial TAM receptor tyrosine kinase AXL (green), IBA1 positive microglia (red), diffuse 6E10 (white) and compact X34 (blue) positive plaque. **(B)** Scatter plots show the immunofluorescence quantitative analysis of AXL-positive percentage of area in the subiculum of 7.5-month-old AD mice (n=6 per group; 3 male and 3 female; 6 experiments). All data are expressed as the mean values ± SEM and analyzed by an ordinary one-way ANOVA and Tukey's multiple comparisons test (*P < 0.05, ***P < 0.001, and ****P < 0.0001). Male mice: •; female mice: o.

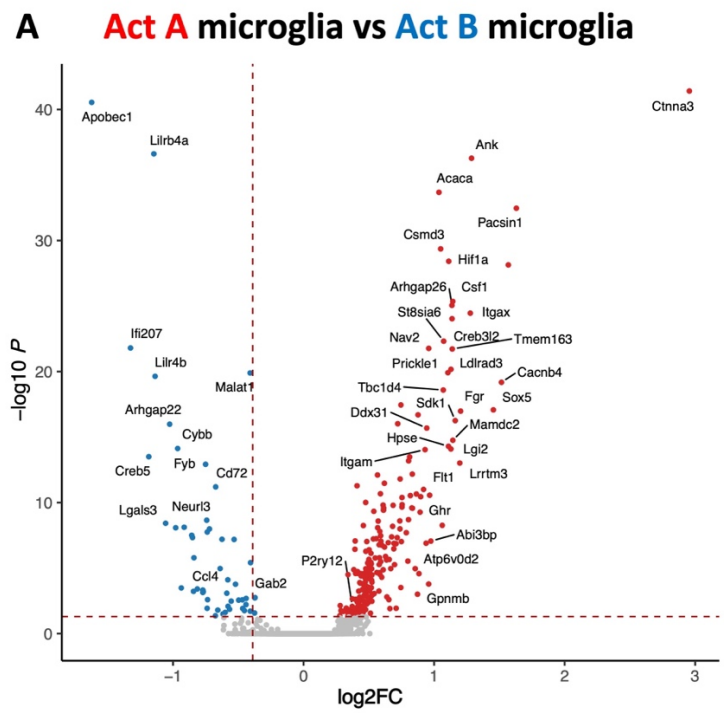

Figure S5. Differentially expressed genes from Act A versus Act B microglia (related to Figure 7)

(A) The volcano plot shows significant DEGs between microglial subclusters, Act A and Act B microglia from single nuclei RNA-seq data.

DEGs *differentially expressed genes*, Act *activated plaque-responsive*

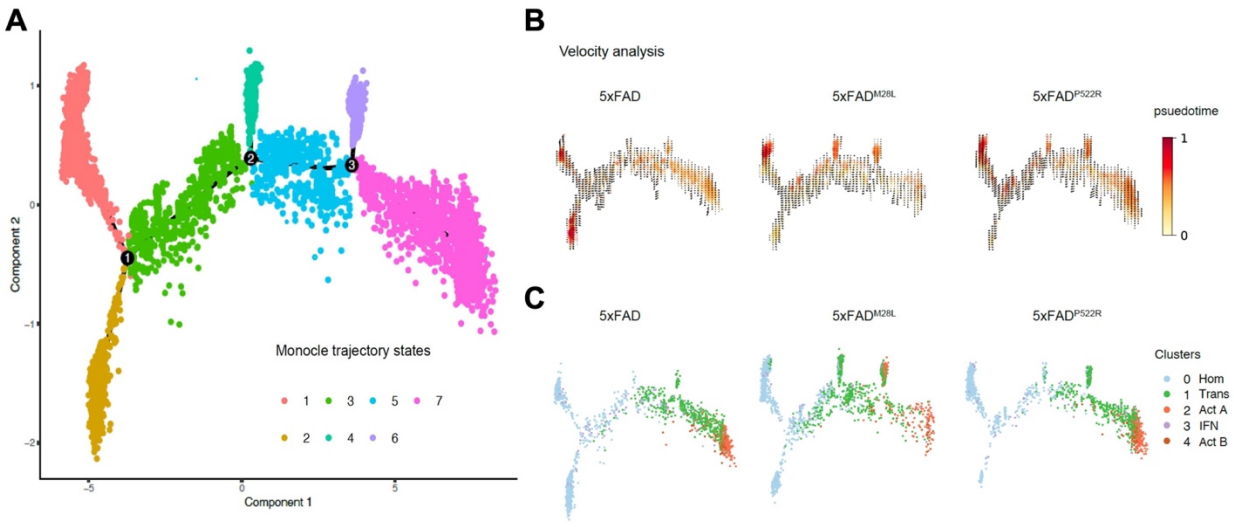

Figure S6. Pseudotime analysis show the trajectory of microglia in AD mice (related to Figure 7)

(A) The pseudotime trajectory inferred from microglial clusters identified 7 monocle states. **(B)** Analysis of RNA velocity, and the nuclei are colored by pseudotime. **(C)** The nuclei are colored by the differentiation state of microglia, including Hom, Trans, Act A, IFN, and Act B.

Hom *homeostatic*, Trans *transitioning*, Act *activated plaque-responsive,* IFN *interferon-responsive*